An integrated method for assessing vulnerability of buildings caused by debris flows in mountainous areas

Chenchen Qiu[1], Xueyu Geng[1]*

[1]School of Engineering, University of Warwick, Coventry, CV4 7AL, UK

Xueyu Geng (**Corresponding Author**):

E-mail: xueyu.geng@warwick.ac.uk

School of Engineering, University of Warwick, Coventry, CV4 7AL, UK

Abstract: The vulnerability assessment of buildings in future scenarios is critical to decrease potential losses caused by debris flows in mountainous areas due to the complex topographical condition that could increase the environmental vulnerability to climate change. However, the lack of reliable methods limits the accurate estimation of physical damage and the associated economic loss. Therefore, an integrated method of physical vulnerability matrix and machine learning model was developed to benefit the estimation of damage degree of buildings caused by a future debris-flow event. By considering the building structures (reinforced-concrete (RC) frame and non-RC frame), spatial positions between buildings and the debris-flow channels (horizontal distance (*HD*) and vertical distance (*VD*)), and impact pressure (P_t) to buildings, a physical vulnerability matrix was proposed to link physical damage with the four factors. In order to overcome the difficulty in estimating the possible impact pressure to buildings, an ensemble machine learning (ML) model (XGBoost) was developed with the involvement of geological factors. Additionally, the *HD* and *VD* were decided based on the satellite images. The Longxihe Basin, Sichuan, China was selected as a case study. The results show that the ML model can achieve a reliable impact pressure prediction because the mean absolute percentage error (MAPE), root mean squared error (RMSE) and mean absolute error (MAE) values are 9.53%, 3.78 kPa, and 2.47 kPa. Furthermore, 13.9% of buildings in the Longxihe Basin may suffer severe damage caused by a future

24   debris-flow event, and the highest economic loss is found in a residential building, reaching 5.1×10^5 €.

25   Overall, our work can provide scientific support for the site selection of future constructions.

26   **Keywords**: Debris flow, geological factors, building, machine learning, vulnerability assessment

1. Introduction

Debris flows are among the most frequent and costly natural hazards due to climate change and difficulty in timely warning (Santi et al., 2011). These events can devastate entire settlements in their path and pose significant threat to natural environment (Immerzeel et al., 2020), causing destruction of aquatic biodiversity, along with damage to properties and finally leading to considerable economic losses worldwide each year (Qiu et al., 2022; Alene et al., 2024; Sridharan et al., 2024). In European Alps, this disaster claimed an economic loss of at least 5 € billion from 1988 to 2012 (Fuchs, 2009; Guzzetti et al., 2005). Moreover, a similar average annual loss is also found in China, approximately 0.17 € billion of annual loss was recorded during the time period of 2005 and 2015 (Miao and Liu, 2020). In this case, a reliable estimation of the potential economic loss caused by debris flows is essential since it can provide guidance for decision-makers about where to place the infrastructures and buildings. The buildings are the most susceptible element to debris flows, and they are responsible for most of the economic loss (Fuchs, 2009; Wei et al., 2018). Therefore, in order to calculate the potential economic loss, it is critical to estimate the damage degree of the buildings since economic loss is linked to the physical vulnerability of a property and its economic value.

The physical vulnerability quantifies the damage degree of a property, and the methods that are used to decide the physical vulnerability include mechanical method (Ruggieri et al., 2023, 2022), vulnerability matrices, vulnerability curves, vulnerability indicators (Papathoma-Köhle et al., 2017). The mechanical methods derive the vulnerability functions of buildings based on numerical models, which may achieve relatively high evaluation accuracy but highly rely on controlled laboratory experiments to obtain input data. As a result, this method itself is time-consuming and costly for regional application (Paudel et al., 2021; Qiu et al., 2022). Three vulnerability curves were derived using numerical modelling to relate the vulnerability to debris-flow intensity, including flow height, flow velocity, and

50 kinematic viscosity (Quan Luna et al., 2011). Although these three curves can suggest the physical

51 vulnerability of a building at risk but fail to consider the impacts of building structures on damage

52 degree. Therefore, a brick structure and a reinforced-concrete frame were included in the development of

53 vulnerability curves by Zhang et al. (2018). However, the involvement of limited building types restricts

54 the application of the curves when the determination of physical vulnerabilities for different building

55 types is required. Therefore, considering the limitations of vulnerability curves, different vulnerability

56 matrixes of buildings have also been developed by many studies due its advantages in interaction

57 understanding between the debris-flow process and elements at risk and easily readable by non-experts

58 (Bründl et al., 2009; Kang and Kim, 2016; Zanchetta et al., 2004). In contrast, these developed matrixes

59 ignored the spatial position (horizontal distance and vertical distance) between the buildings and the

60 debris-flow channels, which would misestimate the damage degree of a building caused by a debris-flow

61 event. As for the vulnerability indicators, this method considers the characteristics of buildings without

62 relating the debris-flow process when evaluating the damage degrees (Fuchs et al., 2019). Therefore, it is

63 crucial to establish a comprehensive assessment matrix that takes into account the structural types,

64 spatial positions between buildings and the debris-flow channels, and debris-flow intensities to estimate

65 the potential damages of the buildings. Additionally, the possible damage degree of the buildings in

66 future scenarios was not considered by the past studies (Papathoma-Köhle et al., 2017). Therefore, this

67 study focuses on conducting an assessment of the potential physical damage of a building due to a future

68 debris-flow event.

69   Among the four factors in deciding the physical damage of buildings (building structure, spatial

70 locations (HD and VD), and impact pressure (P_t)), impact pressure remains an unsolved problem since

71 HD and VD can be determined based on the satellite images. In this case, a machine learning model was

72 developed to predict the impact pressure to a building because this method can uncover intricate and

concealed relationships between various input variables and an output result (Khosravi et al., 2021; Jiang et al., 2023). To leverage the benefits of rapid processing and handling large-scale data, we employ an ensemble model, specifically extreme gradient boosting (XGBoost). This choice is made due to XGBoost's ability to partition data into smaller components, facilitating parallel computation and multithreading to enhance processing speed (Chen and Guestrin, 2016).

In this paper, we proposed an integrated method of physical vulnerability matrix and machine learning model to estimate the physical damage of a building caused by a future debris-flow event, finally estimating the economic loss of this property. The buildings in the Longxihe Basin, Sichuan, Chian, were extracted to conduct a case study to test the efficiency and reliability of this method in physical damage estimation and corresponding economic loss. The formation of terrain in this area is affected by severe tectonic activities, such as earthquakes (Chang et al., 2014; Chang et al., 2015), which can produce abundant loose materials for potential debris flows.

2. Methodology

To estimate the economic loss of buildings caused by a future debris-flow event, several steps are comprised in this study (see Fig. 1):
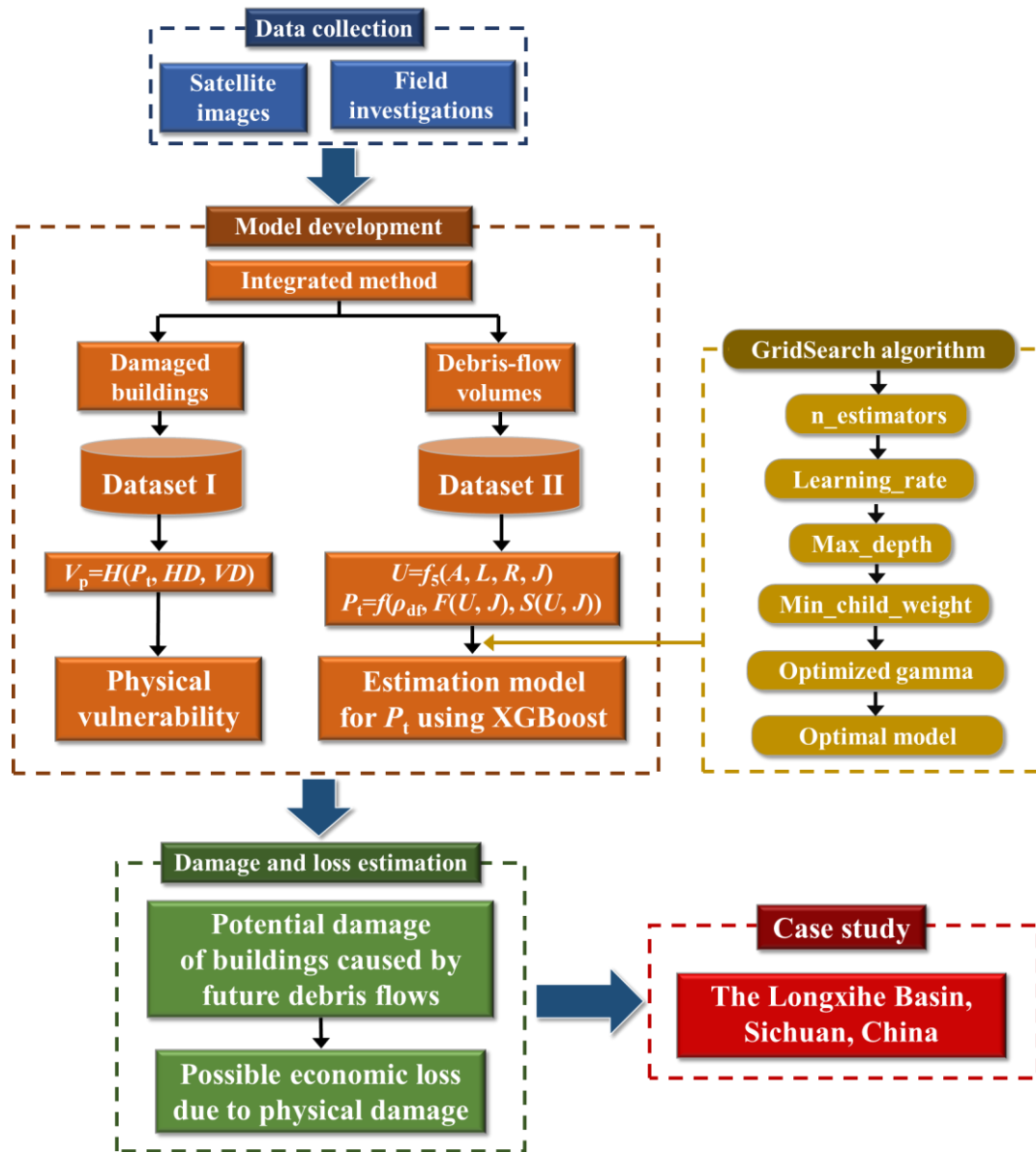
Figure 1. Flow chart of this study

(1) The historical debris-flow events in Gyirong, Tibet Tibetan Autonomous Region, and the Sichuan Basin (Fig. 2) from the past ten years were investigated based on satellite images and field investigations to collect information regarding the debris-flow volumes and damaged buildings.

(2) We categorized the collected historical debris flows into two datasets (dataset I and dataset II) for the development of a physical vulnerability matrix and a prediction model, respectively.

(3) The dataset I includes the debris-flow events that caused damages to the buildings. In detail, V_p is the physical vulnerability of buildings, and P_t represents the impact pressure of a debris-flow event to buildings. HD and VD are horizontal and vertical distance of buildings to their nearest debris-flow

channel. Therefore, this dataset is employed for the development of a physical vulnerability matrix. This

dataset mainly includes the debris-flow events occurred in the Sichuan Basin, China and also several

events in the Gyirong areas.

(4) The dataset II is composed of the debris-flow events that occurred in areas without the

distribution of buildings, and, therefore, no property loss is caused by these events. For the purpose of

establishing an estimation model, a series of factors, such as the depositional volume of a debris-flow

event (U), area of a debris-flow catchment (A), length of the main channel for a catchment (L), the

average topographic relief (R), and the average gradient of main channel (J). ρ_{df} is the mean density of

the material. Therefore, this dataset was used for model training and utilize this model to estimate the

debris-flow intensity in future scenarios, such as debris-flow impact pressure to buildings. This dataset is

shown in Table 6 of Appendix. A.
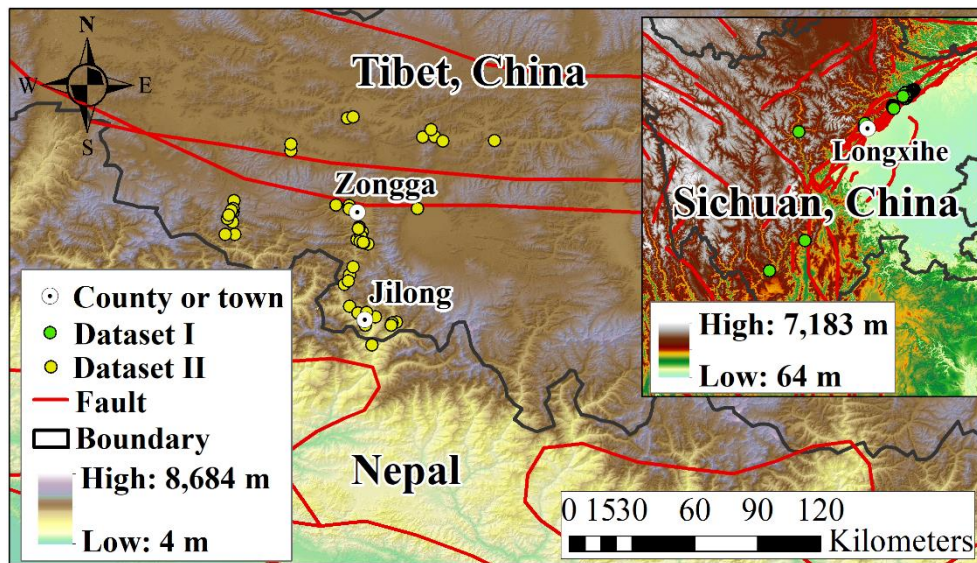
Figure 2. The collected historical debris flows in the Tibet Plateau and the Sichuan Basin

2.1 Physical vulnerability matrix

Vulnerability, usually referring to physical vulnerability, denotes the extent of damage a property

may suffer when subjected to a hazard event, such as a landside and a debris-flow event (Fell, 1994),

ranging from no damage (vulnerability is assigned as 0) to completely destroyed (vulnerability is

115   assigned as 1). To obtain the future economic loss of a building at risk, a physical vulnerability matrix of

116   the buildings was proposed. The determination of physical vulnerability (V_p) relied on the impact

117   pressure (P_t) to buildings, the horizontal distance (HD), and the vertical distance (VD) between the

118   building and the nearest debris-flow channel, as indicated by Eq. (1). The determination details of the

119   three parameters in Eq. (1) are demonstrated in the following sections.

120
$$V_p = H\left(P_t, HD, VD\right) \tag{1}$$

121 **2.1.1 Calculation of impact pressure**

122   In order to propose a physical vulnerability matrix, the first step is to link the impact pressure to

123   damage degree. As suggested by Jakob et al. (2012) and Kang and Kim (2016), P_t can effectively reflect

124   the energy of debris flows and possible damage degree of buildings. However, past studies usually

125   utilized debris-flow magnitude to decide the physical vulnerability since a greater magnitude may

126   indicate a more significant impact force (Dai et al., 2002). This impact force cannot represent the actual

127   damage of a building during a debris-flow event because the catchment with a potential large-scale

128   debris-flow event may not cause severe damage to the buildings. The reason behind this uncertainty

129   could be due to the moderate gradient of debris-flow channel and its frictional resistance, which could

130   decrease the kinetic energy of the travelling mass (Qiu et al., 2024). Consequently, only a slight or

131   moderate damage to buildings could be caused. Therefore, impact pressure can better reflect the damage

132   degree of buildings when subjected to different debris-flow magnitudes, which can be calculated through

133   considering the dynamic overpressure and hydrostatic pressure (Eq. (2)) (Zanchetta et al., 2004):

134
$$P_t = \frac{1}{2}\rho_{df}gh + \rho_{df}v^2 = f\left(\rho_{df}, h, v\right) \tag{2}$$

135   where P_t (kPa) represents the impact pressure to buildings, and g is the gravitational acceleration. v (m/s)

136   represents the flow velocity at the maximum discharge, and ρ_{df} is the mean density of materials for a

137   debris-flow event. h (m) is the flow depth that describes the deposit depth on buildings. As for the

debris-flow velocity (v) at peak discharge (Q_p), it can be calculated using the equation proposed by Rickenmann (1999). This equation considers the debris-flow datasets in different regions, such as Italy, China, Japan, U.S.A, and Columbia, which enables its feasibility to be used in wider and different areas.

$$v = 2.1Q_{\mathrm{p}}^{0.33}J^{0.33} = f_1(Q_p, J) \tag{3}$$

This equation illustrates that the velocity can be decided by Q_{p} (m³/s) and channel gradient (J) (Cui et al., 2013). It's worth noting that J changes along the channel. In our study, we focused on the mean gradient of the main channel within a debris-flow catchment, and it is calculated using the equation proposed by IMHE (1994):

$$J = \frac{\left(\sum_{j=1}^{m}(E_{j-1} + E_j)L_j - 2E_0L\right)}{L^2} \tag{4}$$

where J is the mean path gradient (‰). E_{j} (j=1, 2, …, j-1) represents the elevation of each break point in the movement path (m). Elevation was downloaded from the ASF website (https://search.asf.alaska.edu/#/)) that can provide DEM with a spatial resolution of 12.5 m. L_{j} is length of each section within the movement path (m). m is the number of sections. E_0 represents the elevation at the endpoint of the mass movement (m), while L denotes the length of the travel path (m). The divided sections are presented in Fig. 3.
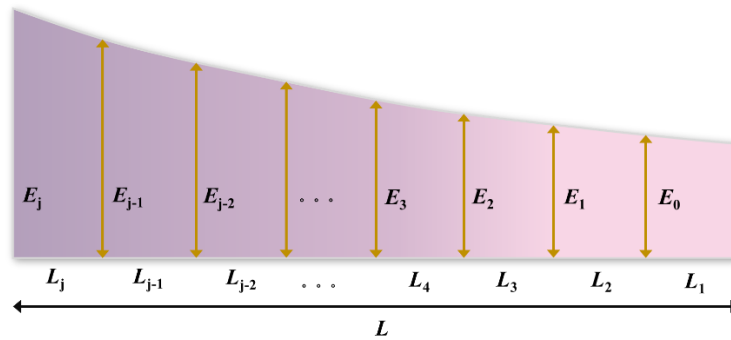
Figure 3. The segments of main channel within a catchment

The calculation of Q_{p} can be determined based on the equation (Eq. (5)):

$$Q_p = (U/152.97)^{1/1.266} = f_2(U) \tag{5}$$

Therefore, the Q_{p} can be calculated based on the estimated volume (U (m³)) of historical debris

flows. However, the absence of flow depth (h) also hampers the calculation of impact pressure. Therefore, an equation is used to calculate the flow depth (Koch, 1998). This formula has been proven to perform well in the numerical simulation of viscous debris flows (Eq. (6)):

$$h = \left(v / C_1 J^{0.5} \right)^{10/3} = f_3 \left(v, C_1, J \right) = f_3 \left(f_1 \left(Q_p, J \right), C_1, J \right) \tag{6}$$

where C_1 represents the dimensional empirical coefficient. This value of parameter is indicated by a semi-theoretical relationship (Eq. (7)) (Rickenmann, 1999):

$$C_1 = 10 Q_p^{2/25} = f_4 \left(Q_p \right) = f_4 \left(f_2 \left(U \right) \right) \tag{7}$$

Therefore, the impact pressure can be described as a function of debris-flow volume and channel gradient, and the impact pressures of dataset I are calculated based on Eqs. (2)-(7) (see Table 1).**2.1.2**

Determination of *HD* and *VD* values

HD and *VD* values were also introduced here since the actual damage will be significant if a building stands close to the debris-flow channel (Sturm et al., 2018). They can be estimated through high-resolution satellite images, such as Gaofen, Ziyuan, WorldView, and GeoEye. In this study, Gaofen-2 satellite images are employed for determining the *HD* and *VD* values. This satellite can capture panchromatic (black and white) images with a spatial resolution reaching 0.8 m and multispectral (color) images with a spatial resolution up to 3.2 m. Therefore, the resolution of satellite images used for determination of *HD* values is 0.8 m. However, there is no elevation information provided by satellite images. Therefore, DEM was used to extract the *VD* information between building and its nearest debris-flow channel. As for the building clusters that are hard to be separated into individual buildings manually, a 'fishnet' tool in GIS was used to automatically divide these clusters into building segments. Furthermore, the rectangle segments were converted into points so that each point represents a building. As a result, the *HD* and *VD* values of a building can be decided. The damaged buildings are mainly distributed on the accumulation fans. Therefore, even though a large *HD* is

observed, the *VD* is small due to the mild slope and smooth topography of the alluvial fans (Marcato et al., 2012). By considering the impact pressure, *HD*, and *VD* values, a physical vulnerability matrix can be established to evaluate the physical damage of a building caused by a debris-flow event.

2.2 Economic loss of a building at risk

The economic loss of a building caused by a debris-flow event can be estimated based on multiplication of its physical vulnerability and economic value.

$$V_e = V_p \times M = H\left(P_t, HD, VD\right) \times M; M = P \times A \tag{8}$$

where V_e and M represent the economic loss and the economic value of a building, respectively. P is the unit price of a building, and A represents the area of a building. Therefore, estimating V_p holds paramount importance in estimating economic loss. However, V_p ($H(P_t, HD, VD)$) is represented by the proposed physical vulnerability matrix. In this context, determining P_t plays a critical role in economic loss estimation. Therefore, to forecast the possible economic loss caused by a future debris-flow event, we need to estimate the impact pressure to buildings caused by a future debris-flow event.

2.3 Prediction model development

To predict the future impact pressure to buildings when a debris-flow event occurs, determining factors is essential. Therefore, we further developed Eq. (6) by integrating Eq. (5) and Eq. (7) to this equation:

$$h = f_3\left(f_1\left(f_2\left(U\right), J\right), f_4\left(f_2\left(U\right)\right), J\right) = F\left(U, J\right) \tag{9}$$

Additionally, Eq. (3) can be rewritten as:

$$v = f_1\left(Q_p, J\right) = f_1\left(f_2\left(U\right), J\right) = S\left(U, J\right) \tag{10}$$

Therfore, the determination of impact pressure reslies on *U* and *J*:

$$P_t = f\left(\rho_{df}, F\left(U, J\right), S\left(U, J\right)\right) \tag{11}$$

However, the debris-flow volume is closely related to a set of geomorphic factors, as suggested by

204   Huang et al. (2020). They are catchment area (A), channel length (L), topographic relief (R), and mean

205   slope of the main channel (J). The catchment area can reflect the debris availability and capacity of

206   generating and containing the volume of loose materials for a debris-flow catchment. As for the channel

207   length, it is related to the entrained and transported sediment volume (Marchi et al., 2019). Therefore,

208   this parameter can also impact the final volume of a debris-flow event. R is defined as the terrain

209   fluctuation and roughness of a catchment. To calculate this value, we need to first decide the optimal

210   statistical unit in this area using the change-point model. Then, the subtraction value between the

211   maximum value and minimum values of an optimal statistical unit is calculated. Finally, we utilized the

212   maximum subtraction value to represent the R value of a catchment. J is defined as the ratio of the

213   elevation difference of the main channel and channel length. A longer distance could be achieved for a

214   debris-flow event if a steep channel exists in a catchment (de Haas and Densmore, 2019). In this case, U

215   can be described as a function of A, L, R, and J:

216
$$U = f_5\left(A, L, R, J\right) \tag{12}$$

217   Furthermore, subsitituting Eq. (12) to Eq. (11):

218
$$P_{\mathrm{t}} = f\left(\rho_{df}, F\left(f_5\left(A, L, R, J\right), J\right), S\left(f_5\left(A, L, R, J\right), J\right)\right) \tag{13}$$

219   Therefore, P_{t} can be described as a complex function of geomorphology-related factors, including A,

220   L, R, and J. To find the complicated correlations among them, an ensemble machine learning model

221   (extreme gradient boosting (XGBoost)) was employed here to establish the relationship and then utilize

222   this relationship to estimate the potential impact pressure to buildings when a future debris-flow event

223   occurs. The basic mechanism of XGBoost is to constantly develop a new decision tree which acts as a

224   weak learner and fits the residual error of the last prediction. After the training of a total of k trees, the

225   final prediction result is the sum of the score of each leaf node in each developed tree. In this study,

226   GridSearch algorithm was employed to decide the optimal hyper-parameters of XGBoost. As a result,

227 the hyper-parameters, such as n_estimators, learning_rate, max_depth, min_child_weight, and gamma,

228 were decided as 500, 0.1, 5, 1, and 0.01, respectively. Overall, the target function of regression is placed

229 in Appendix. A. Additionally, the database II that is used for impact pressure prediction is presented in

230 Table 6 of Appendix. A.

231 **2.4 Model assessment**

232   After the impact pressure prediction, three assessment indexes were used to evaluate the prediction

233 performance, including MAPE (Mean Absolute Percentage Error), RMSE (Root Mean Square Error),

234 and MAE (Mean Absolute Error):

235
$$MAPE = \frac{1}{m}\sum_{i=1}^{m}\frac{\left|y_i - y_{ipre}\right|}{y_i} \tag{14}$$

236
$$RMSE = \sqrt{\frac{1}{m}\sum_{i=1}^{m}\left(y_i - y_{ipre}\right)^2} \tag{15}$$

237
$$MAE = \frac{1}{m}\sum_{i=1}^{m}\left|y_i - y_{ipre}\right| \tag{16}$$

238 where y_i is the actual value, and y_{ipre} represents the prediction value. m is the number of prediction

239 values.

240 **3. Result analysis**

241 **3.1 The relationship between the damage degree and P_t**

242   Fig. 3 shows the different damage degrees of buildings in dataset I. The buildings were classified

243 into two types, including RC-frame (reinforced concrete) and non-RC frame (masonry, wooden structure,

244 and light steel frame). As indicated in Figs. 4(e)-(f), The masonry buildings suffer severe damage, and

245 the light steel frame buildings and wooden structure buildings are destroyed (Figs. 4(g)-(h)) even though

246 the impact pressure to buildings was estimated to be less than 30 kPa. However, the main structure of

247 the reinforced concrete building can stay undamaged (Fig. 4(b)) when severe damage is found on the

248 masonry structure (see a dashed circle in Fig. 4(b)) during the same debris-flow event. This resistance

ability difference indicates the difference in physical vulnerabilities between the RC and the non-RC frames, which can also be seen in Fig. 4(a). Moreover, moderate damage to the RC frame with unreinforced masonry infill walls is found in Fig. 4(c) when a small-scale debris-flow event occurs. Additionally, the RC frame suffers extensive damage when the impact pressure exceeds 100 kPa based on the estimated debris-flow volume. Therefore, the identifications of different damage degrees for buildings provide us with access to proposing a classification standard for the physical vulnerability of buildings.
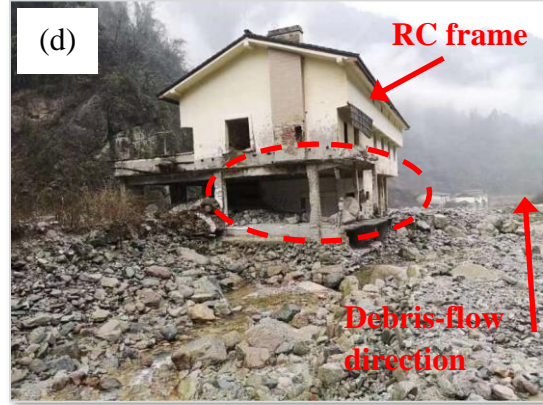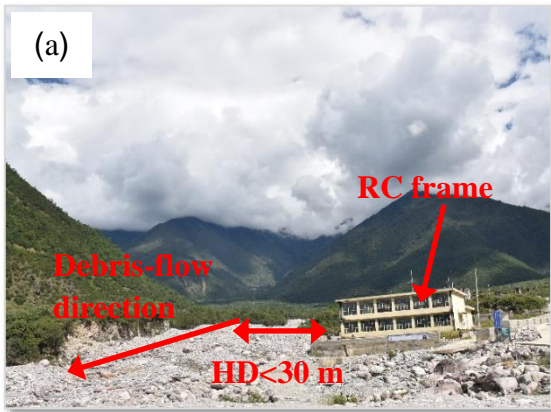
Figure 4. Photographs of the damaged residential buildings caused by debris flows during the field investigations on the Qinghai-Tibetan Plateau

3.2 Determination of *HD* and *VD* thresholds

The field investigations and statistical results show that the non-RC frame buildings are destroyed or suffer structural damage when the *HD* is less than 30 m (Fig. 5(a)). The damaged buildings cannot be repaired, and reconstruction is required. In consistent with the conclusion of past study (Wei et al., 2022), the residential buildings, such as brick structures (Fig. 5(b)) and the RC frame buildings (Fig. 5(c)), are partially buried by the debris-flow sediments without structural damage when the *HD* is greater than 100 m but less than 160 m. Therefore, 160 m is another *HD* threshold to classify the inundated and slightly affected areas. The upper limit of *HD* value for the historical debris flows during the field investigations is 230 m because almost 94% of *HD* values are less than 230 m (see Table 1).

271

272

273
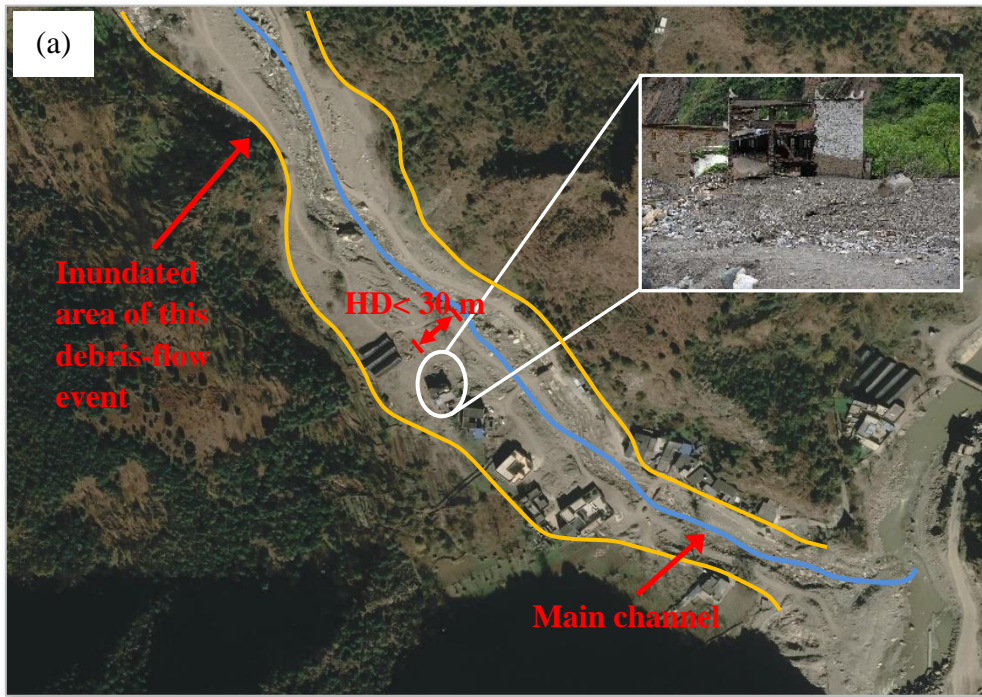
Figure 5. Examples of the determination of the *HD* thresholds

274

Table 1. Dataset I for physical vulnerability matrix.

No.	Year	Lon (°)	Lat (°)	Number of damaged buildings	Impact pressure P_t (kPa)	Maximum *HD* (m)	Maximum *VD* (m)
1	2006	85.3278	28.3735	21	16.1	162	12
2	2007	85.5683	29.1875	13	40.6	141	12
3	2007	85.5528	28.8717	7	37.5	13	7
4	2008	85.6241	29.1869	21	41.0	119	3
5	2010	86.0872	29.1625	11	35.5	54	2
6	2013	85.3112	28.7649	53	24.1	284	29
7	2015	85.2928	28.4174	9	117.4	160	2
8	2015	85.3608	28.4074	22	31.1	131	107
9	2015	85.3542	28.7159	7	17.5	82	13
10	2015	84.7653	28.7559	38	132	74	15

11	2015	85.4566	28.3868	3	5.1	32	10
12	2015	85.4413	28.3827	1	32.7	17	6
13	2015	85.0105	29.1208	3	5.2	133	2
14	2015	85.2579	29.2603	9	9.8	146	2
15	2015	85.2759	29.2652	6	14.8	228	10
16	2015	85.0083	29.1493	4	14.6	171	3

In order to support the thresholds determination of *HD*, we further analyzed the frequencies of *HD* values for the damaged buildings, as depicted in Table 1, through dividing the *HD* values into several intervals. The frequency and accumulative frequency results are shown in Fig. 6.
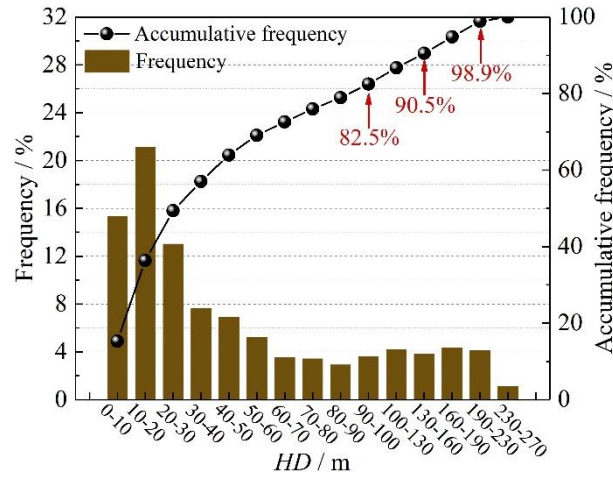
Figure 6. The frequency and accumulative frequency distributions of the 228 damaged buildings.

As depicted in Fig. 6, the highest proportion occurs in the range of 10 to 20 m, accounting for 20.1%, followed by a 15% percentage of *HD* values falling between 20 to 30 m. Therefore, the proportion falling within the range of 0 to 30 m is 49.4%, and approximately 82.5% of the *HD* values is measured under 100 m. Following the suggestion of Liu et al. (2020), a probability of 50% is considered a threshold for debris-flow warning, which implies that 30 m in this study can serve as a threshold. Moreover, the accumulative frequency of 80% is selected as another threshold based on Wei et al. (2018), corresponding to the *HD* value of 100 m. Furthermore, 90.5% of the damaged buildings have *HD* value less than 160 m, and nearly 98.9% of the damaged buildings fall within the *HD* range of 0 to 230 m. As a result, 160 m and 230 m are selected as additional two thresholds. In addition to the determination of *HD* threshold values, the maximum flow depth (h_{max}) in the debris-flow channel is used as a reference to decide the *VD* thresholds since the buildings are mostly situated along the channels (Fig. 5(a) and Fig. 7).

291 Therefore, calculating the elevation difference between the buildings and the nearest debris-flow

292 channel is critical to evaluate the safety of the buildings. It's worth noting that the height of a building

293 was not considered when estimating the *VD* values. For example, both the masonry buildings in Fig. 5(a)

294 and Fig. 7 are close to the debris-flow channel. However, no severe damage is observed for the building

295 in Fig. 7 because it has a considerable vertical distance from the main channel. To decide the *VD*

296 thresholds, the *h* values of the historical debris flows are presented in Table 6 of Appendix. A. The

297 average depth of the debris flows is 2.6 m, and nearly all the *VD* values are less than 4 m. Therefore, 4 m

298 serves as the first threshold, suggesting that the most severe damage to the buildings may be caused

299 when the *VD* is less than 4 m. Whilst a debris-flow depth value of as high as 10 m is suggested (Xie et

300 al., 2013), which can be found in curved channels. Consequently, we utilize 10 m to indicate the

301 moderate damage of buildings when the *VD* is less than 10 m but greater than 4 m. Moreover, a vertical

302 distance of 14 m above the river level is considered to record the river gauging on the Iowa River using a

303 digital video camera (Creutin et al., 2003), which indicates a safe *VD* value to avoid damage caused by

304 the river discharge. Therefore, 15 m is used as the upper limit of the *VD* values in this paper.

305

306 Figure 7**.** Example of the determination of the *VD* threshold, and *VD* in this figure indicates the height

307 difference between the river table and the masonry structure without considering the height of this

308 building.

3.3 Physical vulnerability matrix ($h(P_t, HD, VD)$)

310   The proposed physical vulnerabilities of residential buildings are listed in Table 2. Extensive

311 damage or even complete damage may occur when a non-RC building is located near the debris-flow

312 channel with *HD* less than 30 m and *VD* less than 4 m. However, a significant improvement in resistance

313 ability can be observed when the non-RC frame is replaced by the RC frame considering the same

314 impact pressure, *HD* and *VD* values. In general, the buildings hardly suffer damage when the *VD* is

315 greater than 10 m. Therefore, the economic loss of a building can be calculated based on the proposed

316 physical vulnerabilities and economic values.

317

Table 2. Physical vulnerability matrix

P_t (kPa)	Building structure	*HD*<30 m			30 <*HD*< 100 m		
		4< *VD*	4<*VD*< 10	10<*VD*< 15	4< *VD*	4<*VD*< 10	10<*VD*< 15
<30	RC frame	0.3	0.2	0.1	0.2	0.1	/
	Non-RC frame	0.8	0.7	0.6	0.7	0.6	0.4
30-70	RC frame	0.6	0.5	0.4	0.5	0.4	0.2
	Non-RC frame	1	0.9	0.8	0.9	0.8	0.6
70-100	RC frame	0.7	0.6	0.5	0.6	0.5	0.3
	Non-RC frame	1	1	0.9	1	0.9	0.7
>100	RC frame	0.8	0.7	0.6	0.7	0.6	0.4
	Non-RC frame	1	1	0.9	1	1	0.8
P_t (kPa)	Building structure	100<*HD*<160 m			160<*HD*<230 m		
		4< *VD*	4<*VD*< 10	10<*VD*< 15	4< *VD*	4<*VD*< 10	10<*VD*< 15
<30	RC frame	0.1	/	/	/	/	/
	Non-RC frame	0.6	0.4	0.1	0.4	0.1	/
30-70	RC frame	0.4	0.2	/	0.2	/	/
	Non-RC frame	0.8	0.6	0.3	0.6	0.3	/
70-100	RC frame	0.5	0.3	/	0.3	/	/
	Non-RC frame	0.9	0.7	0.4	0.7	0.4	/
>100	RC frame	0.6	0.4	0.1	0.4	0.1	/
	Non-RC	1	0.8	0.5	0.8	0.5	0.1

3.4 Prediction model development and assessment

The debris flows in Table 6 (see Appendix. A) were divided into a training set and a validation set

with a ratio of 7:3, and the training set is used to train the prediction model. The validation results are

plotted in Fig. 8. Additionally, the performance of the developed model is assessed using the three

indexes (Eqs. (14)-(16)). As indicated in Fig. 8, the prediction results show minor errors to the actual

values, and the MAPE, RMSE and MAE values are 9.70%, 3.98 kPa and 2.74 kPa, respectively. RMSE

value can reflect the extreme errors, and the calculated RMSE value can indicate that there are no

extreme values observed in the prediction results. Additionally, MAPE reflects the error percentage

between the measured and predicted values, and the model is more reliable if the MAPE is closer to 0.

Therefore, it can be concluded that this model performed well in predicting the volume of a future

debris-flow event.
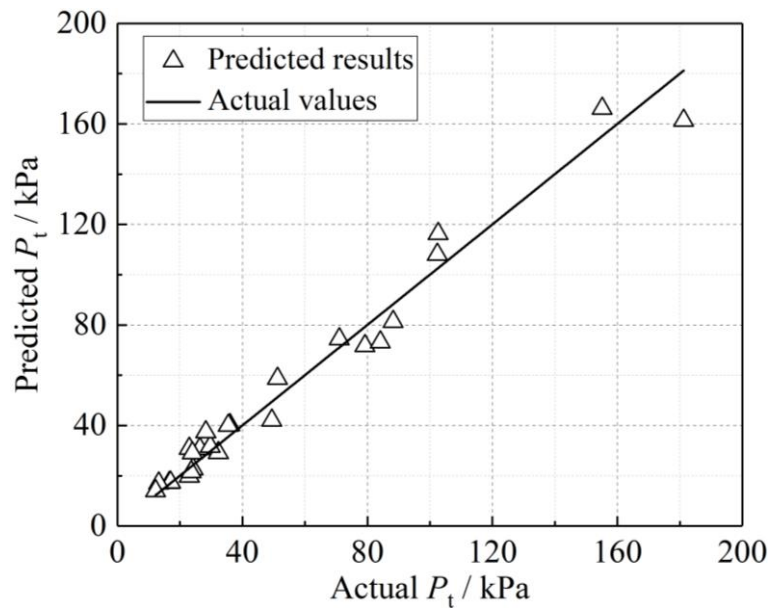
Figure 8. Plots of deviations between the prediction results in hollow triangle estimated by the machine

learning model and actual values represented by a straight line

4 Case study

4.1 Geological setting

We selected the Longxihe Basin (Fig. 9) in Dujiangyan, Sichuan Province, to conduct a case study

(see Fig. 1 about the geographic location of this area), which is 15 km away from the epicenter of the 2008 Wenchuan earthquake. There are three faults crossing this area, namely the Southern Branch of the Yingxiu-Beichuan Fault, the Northern Branch of the Yingxiu-Beichuan Fault, and the Feilaifeng Structure. These faults and structures cause the incised valleys and uplifting of the land surface, resulting in large areas of exposed rocks. Additionally, this study area belongs to the subtropical monsoon climate, with annual precipitation reaching 1,134.8 mm. Over 80 % of the annual rainfall occurs from May to September. Consequently, the abundant rainfall and complex geological structure give birth to frequent debris flows. It was reported that 13 debris-flow events occurred in this basin on 12th May, 24th June, 25th September 2008, and 17th July 2009. In particular, 45 debris-flow events were recorded on 13th August 2010 due to a high-intense rainfall event, causing severe damage to 233 buildings and resulting in the entire economic loss of 7.2×10^7 € (Yu et al., 2011). There are one town and two villages distributed in this basin. The impacts of the Wenchuan earthquake still pose threats to the local people since a time period of at least 20 years is required if the occurrence frequency of debris flows before the earthquake is expected (Yu et al., 2014).
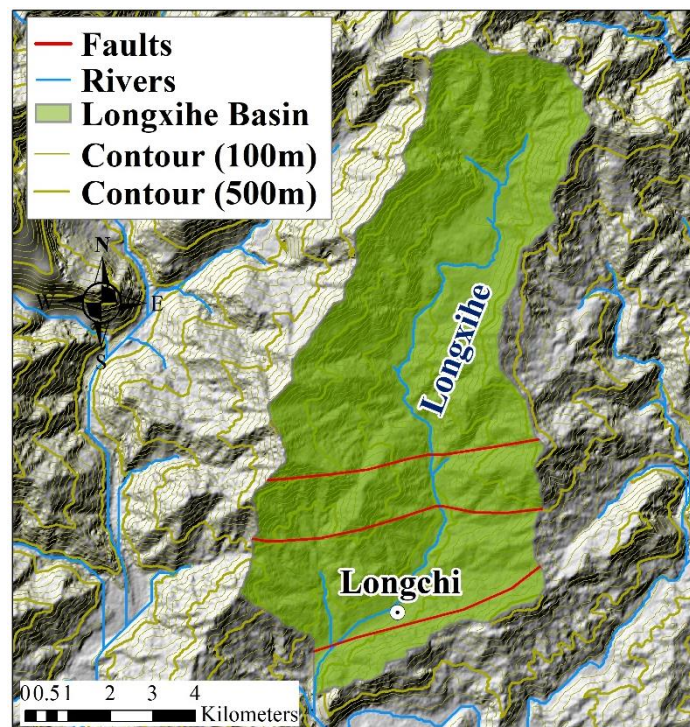
Figure 9. The Longxihe Basin located in north-western part of Dujiangyan, China with a total area of 70.56 km^2 and elevation ranging from 794 m to 3,245 m.

4.2 Estimation of economic loss of buildings

4.2.1 Determination of physical vulnerability

To estimate the potential physical damage of the buildings in the Longxihe Basin, the developed prediction model was applied to predict the potential impact pressure to buildings. As illustrated in Fig. 10(c), the debris-flow catchments within this basin were generated since we mainly focus on the regions with the distribution of buildings and estimate the possible economic loss of the buildings when debris flows occur. Therefore, we extracted a total of 386 buildings in three regions based on the Gaofen-2 satellite images (Fig. 10(a), Fig. 10(b), Fig. 10(d), and Fig. 10(e)). After that, we selected the catchments that are the nearest to the buildings to conduct analysis (see highlighted catchments with red lines in Fig. 10(c)). The input information of these catchments for impact pressure prediction and the predicted results are all listed in Table 3.
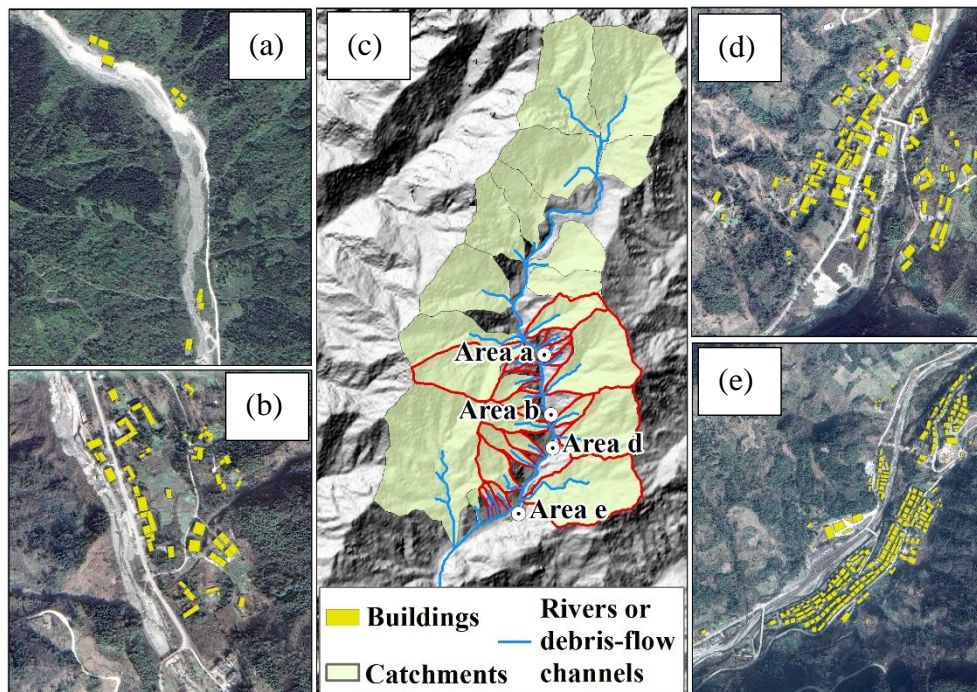
Figure 10. The residential areas (a), (b), (d), and (e) in the Longxihe Basin with highlighted buildings and (c) the debris-flow catchments that were prepared for the establishment of impact pressure

366   estimation model when future debris flows occur

367   Table 3. Prediction results using developed prediction model

No.	A / km^2	L / km	R / m	J	Predicted P_t (kPa)
1	0.4226	0.70	116	0.3024	22.0
2	0.8849	1.00	123	0.3503	26.7
3	0.1447	0.25	113	0.4055	18.0
4	2.9068	0.91	145	0.1668	22.1
5	0.3637	0.58	125	0.2998	19.2
6	0.9317	0.88	130	0.2551	20.9
7	4.1780	1.84	141	0.0751	16.0
8	0.1632	0.61	117	0.3419	19.3
9	0.0932	0.69	112	0.3622	17.3
10	0.1087	0.69	112	0.3542	17.5
11	0.2355	0.73	159	0.6828	16.5
12	1.3027	1.46	145	0.3944	25.2
13	2.8095	1.30	158	0.2466	26.5
14	0.3802	0.89	129	0.4299	19.2
15	0.2177	0.70	136	0.5690	15.8
16	0.1529	0.84	162	0.6821	14.4
17	3.5789	2.23	153	0.3047	33.6
18	0.3179	0.69	127	0.5400	17.4
19	0.1970	0.74	96	0.4056	15.0
20	0.2201	0.90	110	0.4599	13.0

368   In addition to the predicted impact pressures to the buildings by the potential debris flows, the

369   horizontal and vertical distances between each building and the nearest debris-flow channel were

370   measured using GIS. As a result, the physical vulnerabilities of the buildings in Longxihe Basin can be

371   decided based on the proposed physical vulnerability matrix, and the results are shown in Figs. 11(a)-(d).

372

373
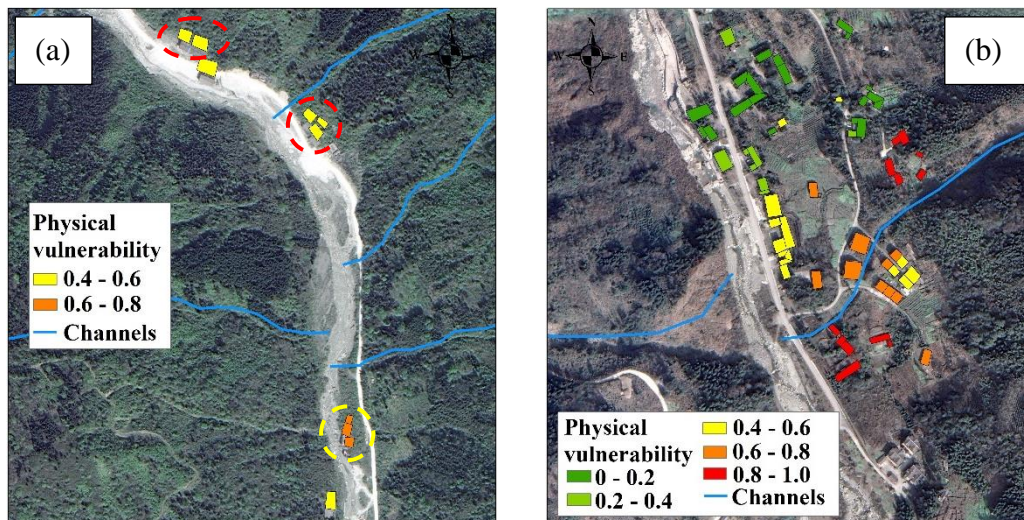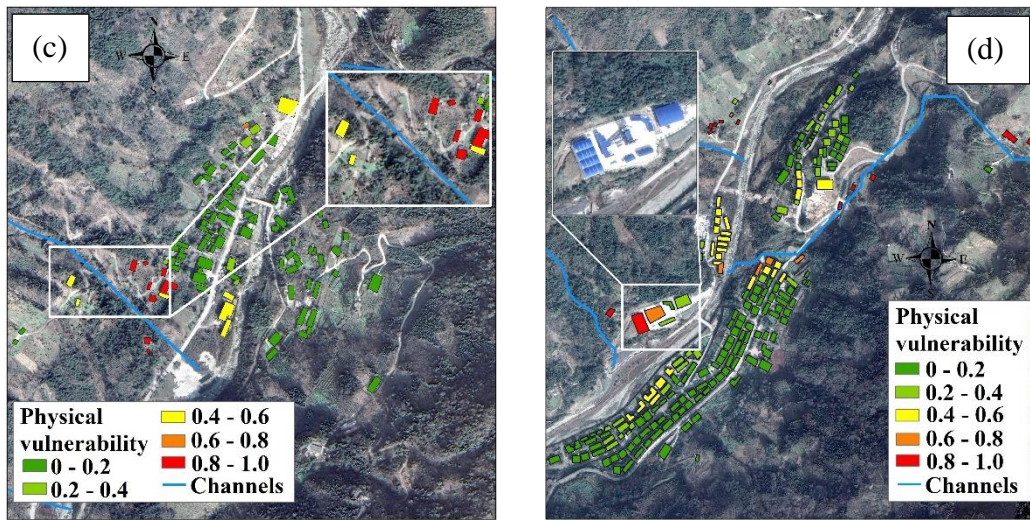
Figure 11. (a)-(d) Physical vulnerabilities of the buildings for residential areas of the Longxihe Basin

corresponding to Figs. 10(a), 10(b), 10(d), and 10(e)

Table 4. Statistical results of the buildings with different physical vulnerabilities

	0 - 0.2	0.2 - 0.4	0.4 - 0.6	0.6 - 0.8	0.8 - 1.0
Number	237	52	45	18	34
Percentage	61.4%	13.5%	11.6%	4.7%	8.8%

The statistical results in Table 4 illustrate that most buildings nearly suffer no damage when a

debris-flow event occurs. This is because these buildings are RC-frame structures, which allow them to

stay undamaged or only suffer slight damage even though they are close to the debris-flow channels.

However, non-RC frame buildings may always suffer severe damage during a debris-flow event if their

locations are near the channels. As indicated in Figs. 11(a)-(d), the buildings with high and very-high

physical vulnerabilities are mainly brick and light steel structures. The difference in resistance ability

allows a greater possibility for RC-frame buildings to keep structures undamaged during the same

debris-flow event when compared to a non-RC building, which is consistent with the field investigation

results in Fig. 4(b). Moreover, a non-RC frame building can also avoid damage even though it is close to

the debris-flow channel. This is because a higher vertical distance to the debris-flow channel can allow

this non-RC building to suffer no damage or light damage. Therefore, a comprehensive analysis by

considering the structure type, spatial distances to debris-flow channel, and potential impact pressure is

significant to establish a reliable physical vulnerability matrix to benefit the determination of the

390   potential damage degree of buildings.

391   In order to validate the efficiency and accuracy of our method in estimating the physical damages of

392   buildings, the damaged buildings caused by debris flows on 13th August 2010 are employed here to

393   assess the reliability of this method. As depicted in Fig. 12(a), the RC-frame buildings suffer a moderate

394   damage (see red dashed circles in Fig. 11(a)) because there are no obvious damages of external or

395   internal walls observed during the field investigations based on the HAZUS building classification

396   scheme (Rojahn, 1988). However, the debris-flow event caused extensive damage (see yellow dashed

397   circles in Fig. 11(a)) to the brick structures due to the partly destroyed external or internal walls (Fig.

398   12(b)). As a result, evacuation of people is necessary and reconstruction is required. Overall, our

399   proposed method can provide a reliable evaluation of physical vulnerability of buildings caused by a

400   debris-flow event and therefore benefit their estimation of economic loss.
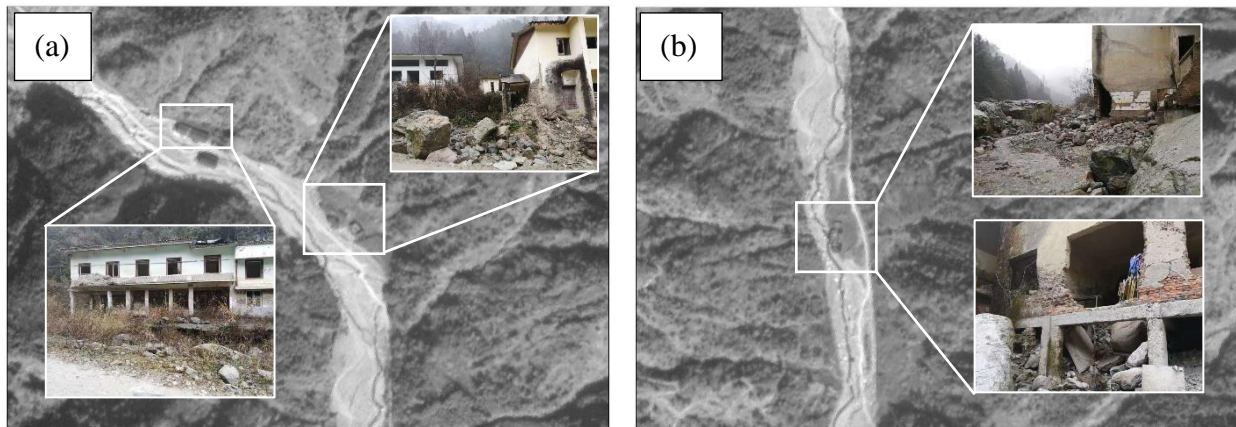
401

402   Figure 12. (a) The RC-frame buildings which suffered moderate damage with no obvious damage of

403   external and internal walls found caused by a debris-flow event on 13 August 2010, and (b) extensive

404   damage was observed on the brick buildings (non-RC frame structure) during the same debris-flow

405   event.

406   **4.2.2 Economic loss**

407   Based on the estimated physical damage, we can further provide a reliable estimation of the

408   economic loss. Six categories of buildings were identified in this study area based on the field

409 investigations. They are residential buildings, factory buildings, office buildings, and livestock houses.

410 Table 5. Unit price (P) of a building in this area

Element	Categories	Unit price	Value based on
Buildings	Residential buildings (RC-frame)	1050.44 €/m²	Average market price
	Residential buildings (Brick structure)	158.38 €/m²	Construction cost
	Business buildings (RC-frame)	1371.47 €/m²	Average market price
	Office buildings (RC-frame)	1050.44 €/m²	\
	Factory buildings (Light steel structure)	237.57 €/m²	Construction cost
	Livestock houses (Brick structure)	7.92 €/m²	Restoration and reconstruction cost

411 The economic value of a residential building in this area is based on the market price, which is

412 provided by the Housing and Urban-rural Construction Agency. As for the unit price of a business

413 building, we refer to the price ratio of a residential building and a business building in the city center of

414 Dujiangyan. The unit price of a business building is normally 30% higher than a residential building. An

415 office building belongs to the national assets, which cannot be rented or sold. However, possible damage

416 still cannot be avoided if a debris-flow event occurs, which therefore requires restoration or

417 reconstruction. Therefore, we refer to the unit price of a residential building to estimate the economic

418 loss of an office building. Unlike the high construction cost and business value of a residential building

419 and a business building, the construction cost of a factory building is low because of its light steel

420 structure. Meanwhile, this kind of building is normally situated at a distance from the city center and

421 residential areas, primarily to mitigate effects of noise and environmental pollution. Most importantly, a

422 factory building invariably occupies a large area, potentially raising the construction cost when situated

423 in the city center due to the exorbitant land prices. Considering the average market price of a factory

424 building, we decide the unit price as 237.57 €/m². Finally, the livestock house is still considered here

425 since two villages are included in the analysis, and the livestock house is built for sheep and cattle.

426 Therefore, the unit price of a livestock building is low (see Table 5). The economic loss of the buildings

427 in the Longxihe Basin are presented in Fig. 13.

428

429
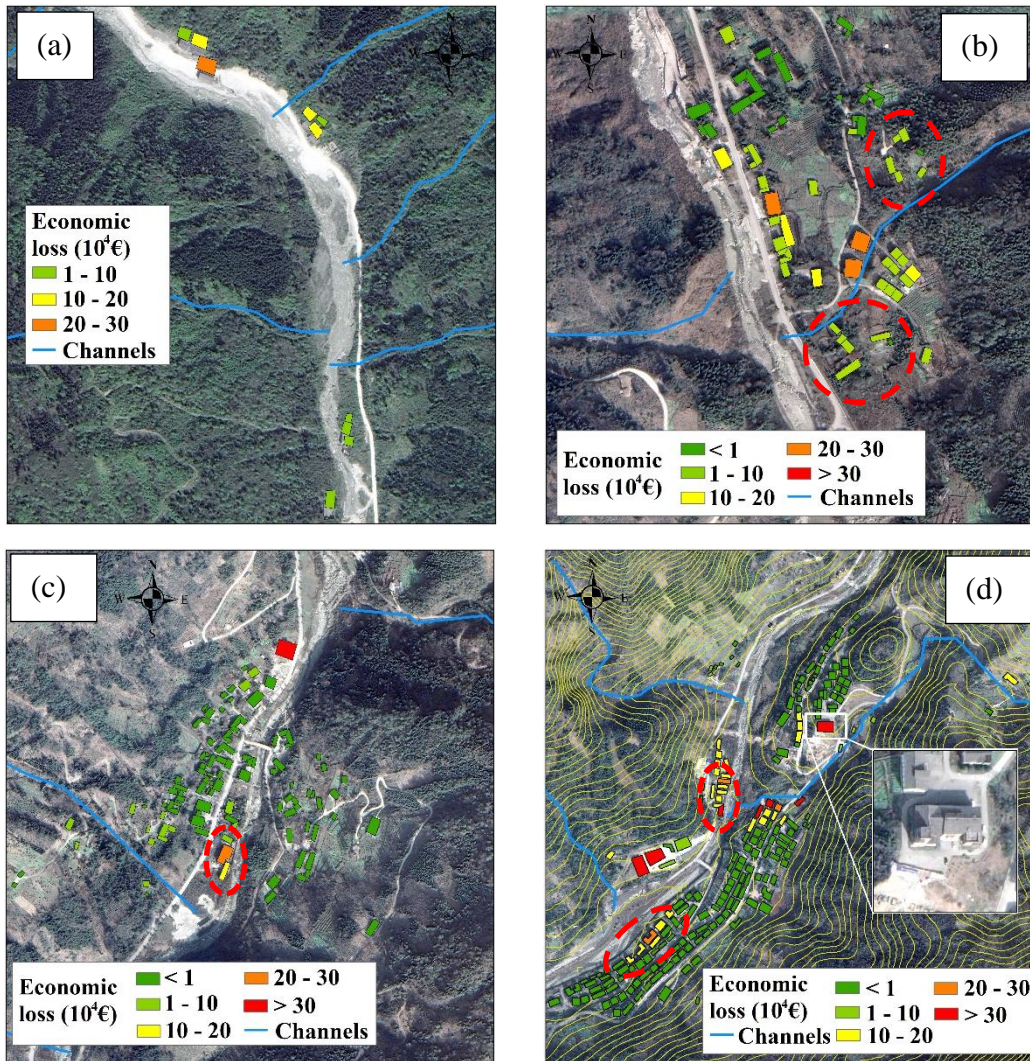
Figure 13. (a)-(d) Estimated economic loss of the buildings for residential areas of the Longxihe Basin corresponding to Figs. 10(a), 10(b), 10(d), and 10(e)

The distribution characteristics of economic loss are different from physical vulnerability. For example, Fig. 11(a) illustrates that the buildings are more likely to suffer severe damage if they are close to the debris-flow channel, especially the non-RC frame structures. However, these non-RC frame buildings require lower reconstruction or restoration costs when compared to the RC-frame buildings (see Fig. 13(a)). In this case, the economic loss is low since it relies on the multiplication of physical vulnerability and economic value of a building (see red dashes in Fig. 13(b)). As indicated in Fig. 13(d), the factory buildings (see Fig. 11(d) and Fig. 13(d)) may suffer an economic loss of $3.2 \times 10^5 €$. As for

439   the reason why a low unit price of a factory building (see Table 5) results in a high economic loss may

440   be due to the large area of this factory building. Therefore, the site selection of a factory building is

441   significant. Although the location of the factory buildings in mountainous areas can avoid noise

442   pollution in urban development and decrease construction costs, the possible economic loss caused by

443   natural hazards cannot be neglected. Additionally, the residential building should not be built on the

444   outlet of the debris-flow catchment directly opposite (see red dash circles in Fig. 13(d)), especially when

445   the foundation of the residential buildings is only slightly higher than the riverway (see yellow contours

446   in Fig. 13(d)). For example, the highest economic loss is found in a residential building (see the image in

447   Fig. 13(d)), reaching 5.1×10^5€. Therefore, at least a 4 m of residential building (RC frame) foundation

448   is essential if the buildings are close to the debris-flow channel based on Table 2. Overall, the analysis of

449   economic loss for buildings in mountainous areas can provide decision-makers with guidance about

450   urban planning.

451   **5. Discussion**

452   The proposed integrated method has been applied for the determination of the damage degree for

453   buildings in the Longxihe Basin, Sichuan, China. The involvement of debris-flow intensities, building

454   attributes, and spatial position between the buildings and debris-flow channel can help to suggest a more

455   reasonable damage degree value caused by debris flows. Specifically, the debris-flow intensity is

456   expressed in impact pressure here, which can indicate the possible consequence of a building if the

457   flowing materials strike the building directly. However, an overestimation of the damage degree may be

458   caused since the spatial positions between the building and debris-flow channel is not a one-dimensional

459   problem. In general, the elevation of a building is greater than that of the debris-flow channel in the

460   horizontal direction. This is because the long-term water flow and historical debris flows move the soils

461   and rocks, causing erosion of the channel bottom and therefore decreasing its elevation. As a result, the

elevation difference between the buildings and the debris-flow channel could cause a loss of impact pressure. Therefore, simply utilizing impact pressure is not enough to reflect the actual damage to a building. In contrast, the introduction of *HD* and *VD* is an effective supplement to improve the estimation of physical damage that the buildings may suffer. Furthermore, the damage degree may vary when subjected to different building structures. In this case, two major types of buildings are considered in this study to distinguish the impact resistance capacities of different building types. Overall, this developed matrix comprehensively describes the factors impacting the damage degree of buildings caused by debris flows.

By utilizing the proposed matrix, we can estimate the damage degree of a building. However, the possible damage in future scenarios is still unclear due to the change in debris-flow magnitude. Therefore, an ensemble machine learning (ML) model is used to predict the volume of a future debris-flow event so that the debris-flow intensities can be calculated based on the empirical relationships. This ML method can effectively avoid over-fitting when training prediction models due to the existence of a regular term. Most importantly, the strong ability in establishing a reliable relationship between a group of independent variables and a dependent variable enables a wider application of ML methods when compared to empirical and regression methods. Therefore, a precise prediction can be expected based on the established relationship using the ML method to indicate the potential damage to buildings caused by a future debris-flow event. However, we are also aware that the current sample size may not support a robustness performance in estimating impact pressure to buildings. For broader applications, continuous input of debris-flow data globally is essential, which may beyond the scope of this study. However, further improvement can also be achieved if the floors of buildings are considered when developing the physical vulnerability matrix. This is because the degree of loss presents a negative correlation with the number of floors (Fuchs et al., 2019). Nevertheless, the limitation cannot alter the fact that our work can

485 benefit the subdivision of buildings in different vulnerability levels and provide suggestions about the

486 site selection of future residential areas.

487 **6. Conclusion**

488   In this paper, an integrated method for vulnerability assessment of buildings caused by future debris

489 flows was proposed. This method includes a physical matrix and a machine learning model, in which

490 this matrix was developed by considering the debris-flow process, building structure, and spatial

491 positions between the buildings and debris-flow channels. To be more specific, the debris-flow process

492 is represented by impact pressure (P_t), which can be estimated based on the debris-flow volume through

493 field investigations. As for the definition of spatial positions, *HD* and *VD* are used to describe the

494 position relation between the buildings and the debris-flow channel. By combining the three parameters,

495 the actual impact pressure on the buildings can be decided. However, the damage degree may vary for

496 different building structures. Therefore, the building structure is further considered to provide a precise

497 estimation of the buildings, including the RC frame and non-RC frame (brick structure, light steel

498 structure, and masonry structure). Therefore, a total of six types of buildings are included in this study.

499 They are residential buildings (*RC* frame and brick structure), business buildings (*RC* frame), office

500 buildings (*RC* frame), factory buildings (light steel structure), and livestock houses (brick structure). At

501 the same time, an ML model (XGBoost) was developed to predict the impact pressure to buildings

502 caused by future debris flows. On the basis of the proposed physical vulnerability matrix and machine

503 learning model, we selected the Longxihe Basin, Sichuan, China, to conduct a case study. The results

504 show that the non-RC buildings may be more likely to suffer severe damage if they are close to the

505 debris-flow channels. The buildings with high and very-high physical vulnerabilities are mainly brick

506 and light steel structures. Consequently, the factory buildings occupy the highest economic loss,

507 reaching 2.41×10^5 € due to their large area. In addition, the buildings may suffer severe economic loss if

they are located the directly opposite of the outlet of the debris-flow catchment. Overall, our studies can

achieve a reliable assessment of the physical damage and corresponding economic loss of buildings and

therefore provide suggestions and scientific support for the future construction planning of buildings.

CRediT authorship contribution statement

Chenchen Qiu: Methodology, Software, Data curation, Writing - Original draft preparation. **Xueyu Geng**: Conceptualization, Visualization, Validation, Supervision, Writing – Review & Editing.

Declaration of competing interest

The authors declare that they have no known competing financial interests or personal relationships that could have appeared to influence the work reported in this paper.

Acknowledgement

This work is financially supported by the European Union's Horizon 2020 research and innovation program Marie Skłodowska–Curie Actions Research and Innovation Staff Exchange (RISE) under grant agreement [grant number 778360].

References

Alene, G.H., Irshad, S., Moraru, A., Depina, I., Bruland, O., Perkis, A. and Thakur, V., 2024. Virtual reality visualization of geophysical flows: A framework. Environmental Modelling & Software, 177, p.106063.

Bründl, M., Romang, H.E., Bischof, N., Rheinberger, C.M., 2009. The risk concept and its application in natural hazard risk management in Switzerland. Nat. Hazards Earth Syst. Sci. 9, 801–813.

Chang, M., Tang, C., Zhang, D.D. and Ma, G.C., 2014. Debris flow susceptibility assessment using a probabilistic approach: A case study in the Longchi area, Sichuan province, China. Journal of Mountain Science, 11, pp.1001-1014.

Chang, M., Tang, C., Ni, H. and Qu, Y., 2015. Evolution process of sediment supply for debris flow occurrence in the Longchi area of Dujiangyan City after the Wenchuan earthquake. Landslides, 12,

534   pp.611-623.

535   Chen, T., Guestrin, C., 2016. XGBoost: A scalable tree boosting system. Proc. ACM SIGKDD Int. Conf.

536   Knowl. Discov. Data Min. 13-17-Augu, 785–794. https://doi.org/10.1145/2939672.2939785

537   Creutin, J.D., Muste, M., Bradley, A.A., Kim, S.C., Kruger, A., 2003. River gauging using PIV

538   techniques: A proof of concept experiment on the Iowa River. J. Hydrol. 277, 182–194.

539   https://doi.org/10.1016/S0022-1694(03)00081-7

540   Cui, P., Xiang, L.Z., Zou, Q., 2013. Risk assessment of highways affected by debris flows in Wenchuan

541   earthquake area. J. Mt. Sci. 10, 173–189. https://doi.org/10.1007/s11629-013-2575-y

542   Dai, F.C., Lee, C.F., Ngai, Y.Y., 2002. Landslide risk assessment and management: An overview. Eng.

543   Geol. 64, 65–87. https://doi.org/10.1016/S0013-7952(01)00093-X

544   Fell, R., 1994. Landslide risk assessment and acceptable risk. Can. Geotech. J. 31, 261–272.

545   Fuchs, S., 2009. Susceptibility versus resilience to mountain hazards in Austria-paradigms of

546   vulnerability revisited. Nat. Hazards Earth Syst. Sci. 9, 337–352.

547   Fuchs, S., Keiler, M., Ortlepp, R., Schinke, R., Papathoma-Köhle, M., 2019. Recent advances in

548   vulnerability assessment for the built environment exposed to torrential hazards: Challenges and the

549   way forward. J. Hydrol. 575, 587–595.

550   Guzzetti, F., Stark, C.P., Salvati, P., 2005. Evaluation of flood and landslide risk to the population of

551   Italy. Environ. Manage. 36, 15–36.

552   Huang, J., Hales, T.C., Huang, R., Ju, N., Li, Q., Huang, Y., 2020. A hybrid machine-learning model to

553   estimate   potential   debris-flow   volumes.   Geomorphology   367,   107333.

554   https://doi.org/10.1016/j.geomorph.2020.107333

555   Immerzeel, W.W., Lutz, A.F., Andrade, M., Bahl, A., Biemans, H., Bolch, T., Hyde, S., Brumby, S.,

556   Davies, B.J., Elmore, A.C. and Emmer, A., 2020. Importance and vulnerability of the world's water

towers. Nature, 577(7790), pp.364-369.

Institute of Mountian Hazards and Environment (IMHE) (1994) Flood, Debris flow, landslide hazard and control. Science Publications. ((in Chinese))

Jakob, M., Stein, D., Ulmi, M., 2012. Vulnerability of buildings to debris flow impact. Nat. Hazards 60, 241–261. https://doi.org/10.1007/s11069-011-0007-2

Jiang, H., Zou, Q., Zhu, Y., Li, Y., Zhou, B., Zhou, W., Yao, S., Dai, X., Yao, H. and Chen, S., 2024. Deep Learning Prediction of Rainfall-driven Debris Flows Considering the Similar Critical Thresholds within Comparable Background Conditions. Environmental Modelling & Software, p.106130.

Kang, H. sub, Kim, Y. tae, 2016. The physical vulnerability of different types of building structure to debris flow events. Nat. Hazards 80, 1475–1493. https://doi.org/10.1007/s11069-015-2032-z

Khosravi, K., Khozani, Z.S., Mao, L., 2021. A comparison between advanced hybrid machine learning algorithms and empirical equations applied to abutment scour depth prediction. J. Hydrol. 596, 126100. https://doi.org/10.1016/j.jhydrol.2021.126100

Koch, T., 1998. Testing various constitutive equations for debris flow modelling. IAHS-AISH Publ. 249–257.

Liu, S., Wei, L., Hu, K., 2020. Topographical and geological variation of effective rainfall for debris-flow occurrence from a large-scale perspective. Geomorphology 358, 107134.

Marcato, G., Bossi, G., Rivelli, F., Borgatti, L., 2012. Debris flood hazard documentation and mitigation on the Tilcara alluvial fan (Quebrada de Humahuaca, Jujuy province, North-West Argentina). Nat. Hazards Earth Syst. Sci. 12, 1873–1882. https://doi.org/10.5194/nhess-12-1873-2012

Miao, C., Liu, X., 2020. Characterization of acceptable risk for debris flows in China: Comparison in debris-flow prone areas and nonprone areas. Int. J. disaster risk Reduct. 42, 101405.

Papathoma-Köhle, M., Gems, B., Sturm, M., Fuchs, S., 2017. Matrices, curves and indicators: A review of approaches to assess physical vulnerability to debris flows. Earth-Science Rev. 171, 272–288.

Paudel, B., Fall, M., Daneshfar, B., 2021. Gis-Based Assessment of Debris Flow Runout in Kulekhani Watershed, Nepal. Geotech. Geol. Eng. 39, 2755–2775. https://doi.org/10.1007/s10706-020-01655-1

Qiu, C., Su, L., Zou, Q., Geng, X., 2022. A hybrid machine-learning model to map glacier-related debris flow susceptibility along Gyirong Zangbo watershed under the changing climate. Sci. Total Environ. 818, 151752. https://doi.org/10.1016/j.scitotenv.2021.151752

Qiu, C., Su, L., Zou, Q., Geng, X., 2022. An AI-based method for estimating the potential runout distance of post-seismic debris flows. International Journla of Disaster Risk Science, pp, 1-14.

Quan Luna, B., Blahut, J., Van Westen, C.J., Sterlacchini, S., Van Asch, T.W.J., Akbas, S.O., 2011. The application of numerical debris flow modelling for the generation of physical vulnerability curves. Nat. Hazards Earth Syst. Sci. 11, 2047–2060. https://doi.org/10.5194/nhess-11-2047-2011

Rickenmann, D., 1999. Empirical relationships for debris flows. Nat. Hazards 19, 47–77. https://doi.org/10.1023/A:1008064220727

Rojahn, C., 1988. Rapid visual screening of buildings for potential seismic hazards: A handbook. Federal Emergency Management Agency.

Ruggieri, S., Calò, M., Cardellicchio, A., Uva, G., 2022. Analytical-mechanical based framework for seismic overall fragility analysis of existing RC buildings in town compartments. Bull. Earthq. Eng. 20, 8179–8216.

Ruggieri, S., Liguori, F.S., Leggieri, V., Bilotta, A., Madeo, A., Casolo, S., Uva, G., 2023. An archetype-based automated procedure to derive global-local seismic fragility of masonry building aggregates: META-FORMA-XL. Int. J. disaster risk Reduct. 95, 103903.

Santi, P.M., Hewitt, K., VanDine, D.F., Barillas Cruz, E., 2011. Debris-flow impact, vulnerability, and response. Nat. hazards 56, 371–402.

Sridharan, A., Gutjahr, G. and Gopalan, S., 2024. Markov–Switching Spatio–Temporal Generalized Additive Model for Landslide Susceptibility. Environmental Modelling & Software, 173, p.105892.

Sturm, M., Gems, B., Keller, F., Mazzorana, B., Fuchs, S., Papathoma-Köhle, M., Aufleger, M., 2018. Understanding impact dynamics on buildings caused by fluviatile sediment transport. Geomorphology 321, 45–59. https://doi.org/10.1016/j.geomorph.2018.08.016

Wei, L., Hu, K., Hu, X., 2018. Rainfall occurrence and its relation to flood damage in China from 2000 to 2015. J. Mt. Sci. 15, 2492–2504.

Wei, L., Hu, K., Liu, J., 2022. Automatic identification of buildings vulnerable to debris flows in Sichuan Province, China, by GIS analysis and Deep Encoding Network methods. J. Flood Risk Manag. 15, 1–18. https://doi.org/10.1111/jfr3.12830

Xie, H., Liu, W., Zhao, J., Hu, K., 2013. Characteristics of Tangjiagou debris flow in Shimian of Sichuan in July 14, 2012. J. Earth Sci. Environ. 35, 90–97.

Yu, B., Ma, Y., Zhang, J.N., Wu, Y.F., Zhang, H.H., Li, L., Chu, S.M. and Qi, X., 2011. The group debris flow hazards after the Wenchuan earthquake in Longchi, Dujiangyan, Sichuan Province. Journal of Mountain Science, 29(6), pp.738-746.

Yu, B., Wu, Y., Chu, S., 2014. Preliminary study of the effect of earthquakes on the rainfall threshold of debris flows. Eng. Geol. 182, 130–135. https://doi.org/10.1016/j.enggeo.2014.04.007

Zanchetta, G., Sulpizio, R., Pareschi, M.T., Leoni, F.M., Santacroce, R., 2004. Characteristics of May 5–6, 1998 volcaniclastic debris flows in the Sarno area (Campania, southern Italy): relationships to structural damage and hazard zonation. J. Volcanol. Geotherm. Res. 133, 377–393.

Zhang, S., Zhang, L., Li, X., Xu, Q., 2018. Physical vulnerability models for assessing building damage

626 by debris flows. Eng. Geol. 247, 145–158.

627

Appendix. A

1. Mechanism of XGBoost

The mechanism of XGBoost is to constantly develop a new decision tree which acts as a weak learner and fits the residual error of the last prediction. After the training of a total of k trees, the final prediction result is the sum of the score of each leaf node in each developed tree. The target function of regression in XGBoost is:

$$L(\phi) = \sum_{i=1}^{m} l\left(y_i, y_i\right) + \sum_{k=1}^{t} \Omega(f_k) \qquad (10)$$

where $\sum_{i=1}^{m} l\left(y_i, y_i\right)$ represents the loss function, and $\sum_{k=1}^{t} \Omega(f_k)$ is the regularisation term. y_i and y_i are prediction value and true value, respectively. m is the number of samples. f_k is the k_{th} tree model. As mentioned above, the newly generated tree needs to fit the residual error of the last prediction, and therefore the prediction result can be presented as:

$$y_i^{t} = y_i^{(t-1)} + f_t(x_i) \qquad (11)$$

Substitute the Eq. (12) into Eq. (11) to rewrite the objective function as:

$$L(\phi) = \sum_{i=1}^{m} l\left(y_i, y_i^{(t-1)} + f_t(x_i)\right) + \sum_{k=1}^{t} \Omega(f_k) \qquad (12)$$

Furthermore, Taylor's second order expansion is introduced to find f_k to minimize the objective function:

$$L(\phi) = \sum_{i=1}^{m} \left[l\left(y_i, y_i^{(t-1)}\right) + g_i f_t(x_i) + \frac{1}{2} h_i f_t^2(x_i) \right] + \sum_{k=1}^{t} \Omega(f_k) + constant \qquad (13)$$

where g_i is the first derivation, and the h_i represents the second derivation

2. Calculation results of impact pressure P_t

Table 6. Dataset II for developing the impact pressure prediction model

No.	A (km²)	L (km)	R (m)	J	P_t (kPa)	No.	A (km²)	L (km)	R (m)	J	P_t (kPa)
1	8.55	3.13	269	0.1051	40.9	42	0.05	0.18	85	0.1908	10.3
2	4.68	1.41	126	0.2162	47.4	43	0.06	0.23	81	0.3038	14.2

3	12.88	4.16	269	0.1246	56.0	44	0.33	0.50	162	0.2792	18.4
4	0.29	0.50	95	0.1638	13.2	45	0.05	0.20	107	0.2661	12.2
5	0.29	0.29	200	0.4122	23.0	46	1.37	1.11	160	0.1763	34.1
6	5.73	0.71	260	0.1175	49.4	47	4.83	1.96	277	0.2071	35.5
7	0.56	0.62	195	0.2475	29.3	48	1.33	0.50	258	0.5117	35.7
8	2.15	0.73	250	0.2736	24.2	49	0.17	0.62	231	0.4727	21.0
9	0.32	0.46	276	0.5452	23.0	50	12.47	3.61	366	0.1853	67.9
10	1.67	0.95	161	0.3699	32.3	51	0.46	0.88	189	0.3819	26.4
11	11.21	1.93	360	0.1512	34.1	52	1.63	1.98	148	0.3115	28.9
12	2.85	1.57	232	0.2568	28.3	53	1.34	1.00	158	0.1727	18.7
13	2.29	1.84	189	0.3581	46.6	54	0.24	0.43	151	0.2867	16.6
14	0.08	0.42	240	0.3561	16.6	55	0.39	0.75	120	0.1745	15.6
15	0.18	0.48	366	0.6976	13.0	56	0.02	0.1	132	0.5295	18.0
16	0.53	0.81	170	0.2943	22.5	57	2.56	1.23	127	0.0998	16.7
17	0.71	1.74	151	0.6494	166.9	58	1.62	0.71	229	0.1673	19.7
18	0.49	1.64	162	0.6494	181.2	59	0.49	1.41	182	0.3000	24.0
19	0.60	1.52	155	0.6469	155.1	60	0.21	0.66	215	0.5384	40.6
20	0.36	1.15	261	0.8214	127.6	61	0.29	1.31	133	0.5184	64.1
21	2.73	2.57	190	0.6771	88.2	62	0.85	1.75	163	0.4578	36.0
22	2.02	2.59	198	0.7028	94.9	63	1.71	2.06	145	0.3879	68.5
23	0.43	1.30	198	0.7729	94.7	64	1.27	2.16	183	0.3522	84.1
24	0.19	1.09	181	0.6873	79.2	65	0.89	2.07	127	0.3385	68.1
25	1.03	2.02	232	0.4369	51.2	66	0.49	1.20	168	0.5681	141.0
26	3.99	3.78	134	0.4061	36.8	67	0.75	1.58	327	0.5566	165.7
27	2.88	2.40	313	0.7107	66.5	68	0.37	0.52	199	0.3404	23.6
28	0.34	1.14	163	0.8571	102.6	69	0.77	0.76	115	0.1566	17.0
29	2.81	2.84	253	0.5250	80.8	70	0.31	0.87	178	0.1317	25.9
30	7.18	4.82	400	0.5139	102.4	71	0.36	0.35	261	0.4578	20.6
31	24.42	9.47	337	0.3153	20.2	72	2.62	1.39	321	0.3482	33.8
32	2.81	1.74	205	0.3191	31.8	73	0.84	1.39	199	0.4899	14.9
33	0.43	1.30	200	0.8012	47.5	74	2.72	2.56	528	0.1069	31.2
34	7.06	4.41	275	0.4473	84.1	75	5.85	0.86	365	0.2962	31.5
35	1.07	2.05	225	0.4431	71.0	76	2.61	1.28	388	0.5317	44.0
36	0.86	2.17	149	0.3979	70.6	77	5.45	2.82	261	0.5228	112.0
37	6.51	2.92	252	0.5029	110.7	78	3.51	0.99	227	0.3839	38.2
38	0.42	1.64	151	0.4813	149.0	79	7.09	2.29	293	0.1962	52.6
39	0.51	1.43	153	0.4899	153.1	80	0.02	0.21	110	0.4390	17.8
40	0.20	0.76	130	0.5520	51.6	81	2.06	1.92	160	0.3211	29.7
41	0.34	1.25	130	0.4942	56.5						

648

649